Received: 11 November 2022 | Revised: 26 June 2023 | Accepted: 23 August 2023

DOI: 10.1111/pce.14711

ORIGINAL ARTICLE

Plant, Cell & Environment PC&E WILEY

Increased activity of core photorespiratory enzymes and CO_2 transfer conductances are associated with higher and more optimal photosynthetic rates under elevated temperatures in the extremophile *Rhazya stricta*

Luke M. Gregory[1,2] | Ludmila V. Roze[1] | Berkley J. Walker[1,2]

[1]Department of Energy-Plant Research Laboratory, Michigan State University, East Lansing, Michigan, USA

[2]Department of Plant Biology, Michigan State University, East Lansing, Michigan, USA

Correspondence
Berkley J. Walker, Department of Energy-Plant Research Laboratory, Michigan State University, East Lansing, MI 48824, USA.
Email: berkley@msu.edu

Funding information
Division of Chemical Sciences, Geosciences, and Biosciences, Office of Basic Energy Sciences of the United States Department of Energy, Grant/Award Number: DE-FG02-91ER20021; National Science Foundation awards from the Division of Integrative Organismal Systems, Grant/Award Number: 2030337

Abstract

Increase photorespiration and optimising intrinsic water use efficiency are unique challenges to photosynthetic carbon fixation at elevated temperatures. To determine how plants can adapt to facilitate high rates of photorespiration at elevated temperatures while also maintaining water-use efficiency, we performed in-depth gas exchange and biochemical assays of the C_3 extremophile, *Rhazya stricta*. These results demonstrate that *R. stricta* supports higher rates of photorespiration under elevated temperatures and that these higher rates of photorespiration correlate with increased activity of key photorespiratory enzymes; phosphoglycolate phosphatase and catalase. The increased photorespiratory enzyme activities may increase the overall capacity of photorespiration by reducing enzymatic bottlenecks and allowing minimal inhibitor accumulation under high photorespiratory rates. Additionally, we found the CO_2 transfer conductances (stomatal and mesophyll) are re-allocated to increase the water-use efficiency in *R. stricta* but not necessarily the photosynthetic response to temperature. These results suggest important adaptive strategies in *R. stricta* that maintain photosynthetic rates under elevated temperatures with optimal water loss. The strategies found in *R. stricta* may inform breeding and engineering efforts in other C_3 species to improve photosynthetic efficiency at high temperatures.

KEYWORDS

catalase, CO_2 transfer conductance, phosphoglycolate phosphatase, photorespiration, *Rhazya stricta*, water-use efficiency

1 | INTRODUCTION

Global warming has increased the frequency of high-temperature events that place physiological constraints on C_3 photosynthetic performance. This warming is happening rapidly; the most recent IPCC report estimates global surface temperatures will increase by 1.4°C–4.8°C in the next century, meaning that future plants will experience higher temperatures than they have experienced in at least the last 100 000 years (Pörtner et al., 2022). Increasing global surface temperatures will raise air temperature and alter atmospheric vapour pressure differential (VPD), which directly influences various physiological processes in plants (Moore et al., 2021). These physiological processes include enzymatic temperature response, leaf energy balance, stomatal behaviour, cell membrane properties, and changes in photosynthetic performance (Larkindale & Huang, 2004; Marcum, 1998; Moore et al., 2021; Prasertthai et al., 2022; Urban et al., 2017a, 2017b). While all these physiological processes are important, photosynthetic performance under future climates is of particular interest due to its participation in the global carbon cycle and recent efforts to improve its efficiency (De Souza et al., 2022; Kromdijk et al., 2016; South et al., 2018). Photorespiration and intrinsic water use efficiency (*WUE*) will disproportionately affect C_3 species as temperatures increase since they lack the carbon-concentrating mechanism of C_4 or CAM species. Understanding how C_3 species will manage higher photorespiratory fluxes and optimise *WUE* at elevated temperatures will help us resolve temperature-dependent mechanisms and likely advance breeding and engineering strategies in C_3 species.

Increased photorespiration limits C_3 photosynthetic performance at elevated temperatures. The photorespiration pathway begins when O_2 binds to ribulose-1,5-bisphosphate carboxylase/oxygenase (rubisco) instead of CO_2. The resulting oxygenation of ribulose-1,5-bisphosphate (RuBP) produces 3-phosphoglycerate (3-PGA), a C_3 cycle intermediate, and 2-phosphoglycolate (2-PG), an intermediate that inhibits the C_3 cycle enzymes triose phosphate isomerase and sedoheptulose-1,7-bisphosphatase (Anderson, 1971; Flügel et al., 2017). To reduce the inhibition of the C_3 cycle enzymes, photorespiration detoxifies and recycles 2-PG back into 3-PGA through a set of reactions that occur in the chloroplast, peroxisome, mitochondrion, and cytosol (see Box 1). Although the photorespiratory pathway is an effective solution to handle RuBP oxygenation, it lowers the efficiency of photosynthesis by reducing net carbon fixation by releasing CO_2 (Bauwe et al., 2012). Relative rates of RuBP oxygenation increase with temperature due to decreases in rubisco specificity and decreased solubility of CO_2 relative to O_2 (Hall & Keys, 1983; Hermida-Carrera et al., 2016; Jordan & Ogren, 1984). Therefore, under elevated temperature, greater oxygenation rates will increase rates of 2-PG production that need to be detoxified and recycled by the photorespiratory pathway.

While rubisco kinetics and gas solubilities determine the rate at which 2-PG is initially produced following rubisco oxygenation, the temperature response of downstream photorespiration and the effects on subsequent CO_2 loss is unclear. Loss of CO_2 occurs through the decarboxylation of glycine in the mitochondrion; however, there is evidence for additional release of CO_2 from non-enzymatic decarboxylation reactions that occur within the peroxisome, especially under elevated temperatures (Abadie et al., 2016; Bao et al., 2021; Somerville & Ogren, 1980; Somerville, 2001; Walker & Cousins, 2013). The $CO_{2released}$ from nonenzymatic decarboxylation reactions combined with CO_2 loss from GDC would reduce net carbon fixation.

Another challenge to maintaining C_3 photosynthetic performance at elevated temperatures is preserving plant water. The driving

BOX 1

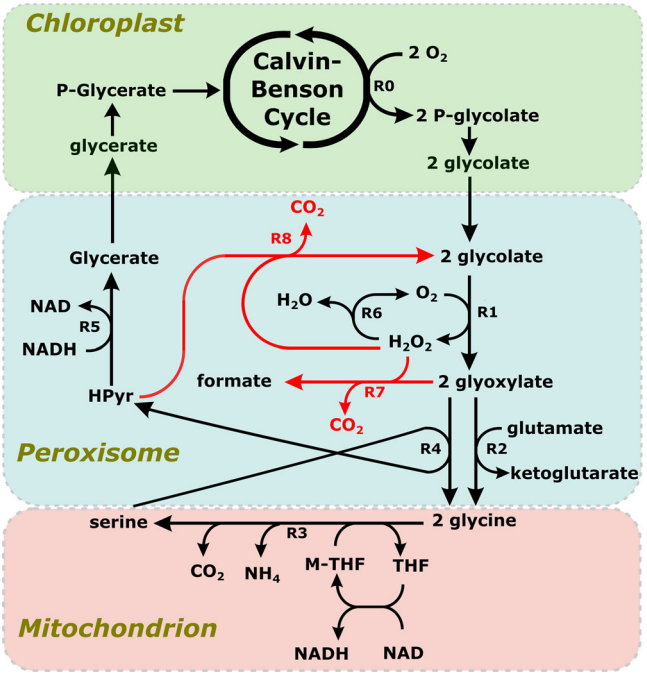

Following the oxygenation of RuBP by rubisco in the chloroplast, phosphoglycolate phosphatase (PGP) converts 2-PG into glyoxylate. Glycolate in transported to the peroxisome where glycolate oxidase (GO) catalysers the conversion of glycolate and O_2 to glyoxylate and hydrogen peroxide (H_2O_2). H_2O_2 is decomposed in the peroxisome into H_2O and O_2 by catalase (CAT), while glyoxylate is animated with glutamate or alanine to produce glycine via aminotransferase (GGAT or AGAT). Glycine in transported into the mitochondrion and decarboxylated to produce serine by glycine decarboxylate complex and serine hydromethyltransferase. Serine is transported back to the peroxisome and converted to hydroxypyruvate by serine glyoxylate aminotransferase (SGAT). hydroxypyruvate is reduced by hydroxypyruvate reductase (HPR) to form glycerate. Glycerate is transported back to the chloroplast and catalysed by glycerate kinase (GLYK) to 3-PGA, which re-enter the C_3 cycle. Image reproduced from: CAT protects against nonenzymatic decarboxylations during photorespiration in *Arabidopsis thaliana*, Bao et al., Plant Direct Volume 5 Issue 12. Copyright (c) [2021] authors hold copyright and have given permission to reproduce.

force of water vapour loss or transpiration from the plant to the atmosphere is VPD. VPD, which is the difference in water vapour partial pressure between the intercellular airspace of the leaf and the atmosphere, responds to air temperature. As temperatures rise, VPD increases curvilinearly and drives greater transpiration rates (Lawrence, 2005). The greater rates of transpiration alter CO_2 and H_2O exchange between plants and the atmosphere and cause a greater water loss per carbon assimilated (or reduction in *WUE*) because CO_2 and H_2O exchange through the same stomatal pore (Rawson et al., 1977). While the stomatal conductance (g_{sw}) constrains CO_2 and H_2O exchange with the atmosphere and the intercellular airspace, mesophyll conductance (g_m) constrains only the transfer of CO_2 from the intercellular airspace to the site of carboxylation without a corresponding loss of H_2O. Given the ability of g_m to facilitate CO_2 transfer without accompanying H_2O loss, it is unclear to what degree plants adapted to high temperatures have exploited this property to limit water loss while maximising CO_2 availability. The reduction of CO_2 availability through regulated decreases in g_{sw} is large enough to decrease photosynthetic performance in C_3 plants, which lack a carbon concentrating mechanism.

Does C_3 photosynthetic performance always decrease with increasing temperatures, or have some C_3 species adapted to facilitate high rates of photorespiration while maintaining photosynthesis and *WUE* at elevated temperatures? To explore this question, we investigated how *Rhazya stricta*, a C_3 desert extremophile, has adapted to maintain photosynthetic performance at elevated temperatures. *R. stricta* is ideal for studying heat adaptation as it is native to hot-arid environments. Past work suggests that *R. stricta* has distinct physiological adaptations to extreme temperatures (Lawson et al., 2014; Yates et al., 2014). For example, leaf temperature during in situ diurnal measurements of *R. stricta* climbed from 26°C to 43°C with an accompanying increase in photorespiration (Lawson et al., 2014). During this increase in temperature, the relative water content in the leaf was stable, suggesting there was minimal water stress.

In this paper, we determine how *R. stricta* facilitates high rates of photorespiration while maintaining photosynthesis and *WUE* at elevated temperatures. Here, we hypothesise that *R. stricta* maintains photorespiratory capacity at elevated temperatures through increased activity of key photorespiratory enzymes. We additionally hypothesise that *R. stricta* optimises *WUE* by favoring g_m relative to g_{sw} under elevated temperatures. To test these hypotheses, we compared various physiological and biochemical parameters in two species, *Nicotiana tabacum*, a thermotolerant C_3 species, and *R. stricta*, an extremophilic C_3 species. The results from these measurements indicate that *R. stricta* maintains higher rates of photorespiration than *N. tabacum* under moderate and elevated temperatures and that these higher rates of photorespiration correlate with increased activity of key photorespiratory enzymes; phosphoglycolate phosphatase (PGP) and catalase (CAT). Additionally, the g_{sw} and g_m appear to be optimised for water-use efficiency but not necessarily photosynthetic carbon gain to temperature in *R. stricta*. These results suggest important adaptive strategies in *R. stricta* that maintain photosynthetic rates under elevated temperatures with optimal water loss. (Table 1)

2 | MATERIAL AND METHODS

2.1 | Plant material and growth conditions

R. stricta seeds were wild collected for this study and are available through the Millennial Seed Bank coordinated by the Royal Botanical Gardens, Kew Serial number 220547. Before planting, *R. stricta* seeds were surface-sterilised inside a Laminar hood with 100% ethanol for 5 min followed by a 7-min soak in 25% bleach solution. Seeds were then washed and vortexed three times in deionized water. After sterilisation, seeds germinated in a petri dish filled with deionized water for 2-weeks. During the 2 weeks, water was changed as needed to remove yellow exudate to avoid possible allelopathic inhibition of germination. Seeds were transferred when roots emerged and were 1 cm in length to 11.36 L pots containing half Sure-Mix potting soil (Michigan Grower Products, Inc.) and half sand mixture. *R. stricta* were grown for an additional 8 weeks until leaves were large enough for gas exchange measurements. *N. tabacum* were sown and grown in 0.7 L pots containing Sure-Mix potting soil (Michigan Grower Products, Inc.) for 4–6 weeks until leaves were large enough for gas exchange measurements. Both *R. stricta* and *N. tabacum* plants were grown in a greenhouse with an average day/night temperature of 34/27°C and a 16/8 photoperiod of supplemental light (150 µmol m^{-2} s^{-1}). Plants were watered as needed with ½-strength Hoagland's solution.

2.2 | Estimating C_i^* and R_L using the common intersection method

Gas exchange was measured on the youngest, fully expanded leaves of *R. stricta* and *N. tabacum* using a LI-6800 (LI-COR Biosciences) using a 9 cm^2 chamber with 50:50 blue:red LEDs to better replicate the blue-to-red ratio of the solar spectrum at the earth's surface. To shift between temperatures ranging from 20°C to 40°C, the LI-6800 was placed inside a climate-controlled chamber (Percival Scientific). The apparent CO_2 compensation point uncorrected for g_m (C_i^*) and rates of CO_2 release from non-photorespiratory processes in the light (R_L) were measured using the common intersection method (Laisk, 1977; Walker et al., 2016a). During the measurement, steady-state *A* was measured at 3, 5, 7, 9, 11, and 40 pascal (Pa) CO_2 under various light intensities (250, 165, 120, 80, and 50 µmol PAR m^{-2} s^{-1}), with a flow rate of 500 µmol s^{-1}. Linear fits of the CO_2 response curves were made for each light intensity. A linear regression of the slope-intercept from these linear fits was used to estimate C_i^* and R_L.

TABLE 1 Parameter definitions.

Parameter	Biological description	Unit
A	Net CO_2 assimilation rate	μmol m^{-2} s^{-1}
C_a	The CO_2 partial pressure in the ambient air	Pa
C_i	The CO_2 partial pressure in the intercellular airspace of the leaf	Pa
C_i^*	The CO_2 partial pressure in the intercellular airspace of the leaf at the photorespiratory compensation point	Pa
C_c	The CO_2 partial pressure in the chloroplast	Pa
g_{sw}	Stomatal conductance to H_2O in air	mol m^{-2} s^{-1}
g_{tc}	Stomatal conductance to CO2 in air	mol m^{-2} s^{-1}
g_m	Mesophyll conductance to CO_2	μmol m^{-2} s^{-1} Pa^{-1}
J_{max}	Maximum rate of electron transport	μmol m^{-2} s^{-1}
Lg_{tc}	Limitation imposed by stomatal conductance on net CO_2 assimilation rate	%
Lg_m	Limitation imposed by mesophyll conductance on net CO_2 assimilation rate	%
$S_{c/o}$	specificity of rubisco for CO_2 relative to O_2	Unitless
R_L	Non-photorespiratory CO_2 release in the light	μmol m^{-2} s^{-1}
v_c	The velocity of rubisco carboxylation	μmol m^{-2} s^{-1}
$v_{c,max}$	The maximum velocity of rubisco carboxylation	μmol m^{-2} s^{-1}
v_o	The velocity of rubisco oxygenation	μmol m^{-2} s^{-1}
v_o/v_c	The velocity of rubisco oxygenation per carboxylation	Unitless
Γ^*	The CO_2 partial pressure in the chloroplast at the photorespiratory compensation point	Pa
α	Stoichiometric release of CO_2 per oxygenation reaction	mol mol^{-1}
Δ_f	Discrimination associated with photorespiration	‰
f	$^{12}C/^{13}C$ fractionation during photorespiration	‰
Φ_{CO2}	Maximum quantum yield of CO_2 fixed per photon absorbed	Unitless

2.3 | Measuring g_m with gas exchange and ^{13}C isotope discrimination

g_m was measured using in vivo gas exchange combined with online measurements of the carbon isotope discrimination method with our particular system as described previously (Fu et al., 2023). Briefly, gas exchange was performed as above using an LI-6800 with 9 cm^2 chamber with 50:50 blue:red LEDs. To measure carbon isotope discrimination, the LI-6800 was coupled to a tunable infrared laser differential absorption spectrometer (TILDAS-CS, Aerodyne Research). The CO_2 in the leaf chamber, flow rate, and irradiance were set to 40 Pa CO_2, 300 μmol s^{-1}, 1750 μmol PAR m^{-2} s^{-1}, respectively. Measurements were made under 2% O_2 to minimise uncertainties about precise photorespiratory fractionation (f) values and since g_m has not been shown to be oxygen dependent (further validated below). To measure under 2% O_2, N_2 and O_2 were mixed by mass-flow controllers (Alicat Scientific, Inc.). For calibrating the $\delta^{13}C$ values, a reference line was supplied with isotopically characterised CO_2 ($\delta^{13}C$ vs. VPDB: −4.6 ± 0.3‰; Airgas Specialty Gases). Leaves were measured after reaching steady-state assimilation rate (A) at each temperature, starting at 20°C and increasing to 40°C, by 5°C steps. g_m was calculated from carbon isotope equations presented previously (Ubierna et al., 2018) that build upon foundation work in isotope-ration mass spectroscopy-based approaches in isotope discrimination (Evans et al., 1986; Farquhar & Cernusak, 2012; Farquhar et al., 1982) and the recent advances in online methods using tunable diode lasers (Barbour et al., 2007; Tazoe et al., 2011; von Caemmerer & Evans, 2015).

2.4 | Measuring the temperature response for photorespiratory discrimination and fractionation

Photorespiratory discrimination (Δ_f) and the $^{12}C/^{13}C$ fractionation during photorespiration (f) for *R. stricta* and *N. tabacum* were resolved using the in vivo gas exchange combined with online measurements of the carbon isotope discrimination (described above). Leaves were measured at 25°C and 35°C, both at 2% and 21% oxygen. g_m was

determined at 2% oxygen where photorespiratory release of CO_2 was minimised assuming $f = 11.8‰$ (with the corresponding rubisco ^{13}C fractionation; 30‰) (Tcherkez, 2006; Ubierna et al., 2018). We then assumed the g_m measurements at 2% oxygen were the same as the g_m at 21% oxygen to solve for Δ_{gm} at both measuring temperatures. g_m was also determined assuming $f = 11.8‰$ for both oxygen concentrations for each temperature. We could calculate Δ_f using:

$$\Delta_f = \Delta_i - \Delta_o - \Delta_{gm} - \Delta_e \quad (1)$$

Then, with Δ_f, derive f by:

$$f = \frac{1 - t}{1 + t}\frac{\alpha_e}{\alpha_f}\Delta_f\frac{C_a}{A} \quad (2)$$

(Evans & von Caemmerer, 2013; Ubierna et al., 2018).

2.5 | Calculating Γ^*

Γ^* in *R. stricta* and *N. tabacum* was calculated using C_i^*, R_L and g_m. Γ^* was determined according to

$$\Gamma^* = C_i^* + \frac{R_L}{g_m} \quad (3)$$

(Von Caemmerer, 2000). To account for internal dependency on solved parameters, g_m and Γ^* were re-solved iteratively using previous g_m, and Γ^* values; iterations continued until there was negligible change in re-solved g_m, and Γ^*.

2.6 | Estimating rates of v_c and v_o

v_c and v_o for *R. stricta* and *N. tabacum* were estimated according to

$$v_c = \frac{A + R_L}{1 - \Gamma^*/C_c} \quad (4)$$

$$v_o = \frac{v_c - A - R_L}{0.5} \quad (5)$$

(Walker et al., 2020), where, the partial pressure of CO_2 at the site of rubisco catalysis (C_c) was determined by

$$C_c = C_i - \frac{A}{g_m}. \quad (6)$$

2.7 | Finding saturating light intensity and maximum quantum yield

Gas exchange was measured on the youngest, fully expanded leaves of *R. stricta* and *N. tabacum* using a LI-6800 (LI-COR Biosciences) using a 6 cm^2 chamber with 50:50 blue:red LEDs. During the measurement, steady-state A was measured at 40 Pa CO_2 under monotonically decreasing light intensities (2000, 1500, 1000, 750, 500, 350, 250, 150, 75, 50, 45, 40, 35, 30, 25, 20, 15, 10, and 5 µmol PAR m^{-2} s^{-1}) with a flow rate of 500 µmol s^{-1}. The leaf absorptivity in *R. stricta* and *N. tabacum* leaves was measured using a SpectroClip-JAZ-TR integrating sphere (Ocean Optics Inc.) and used to calculate absorbed quanta. To find maximum quantum yield of CO_2 fixed per photon absorbed, the relationship of assimilation to absorbed quanta was then fit to a linear regression at low light intensity.

2.8 | Measuring $v_{c,max}$ and J_{max} with the dynamic assimilation technique

Gas exchange was measured on the youngest, fully-expanded leaves of *R. stricta* and *N. tabacum* using a LI-6800 (LI-COR Biosciences) with a 6 cm^2 chamber with 50:50 blue:red LEDs. To shift between temperatures ranging from 20°C to 40°C, the LI-6800 was located inside of a climate-controlled chamber (Percival Scientific). Range matching and dynamic calculations were preformed according to manufacturer's instructions. CO_2 response curves for fitting maximum rate of rubisco carboxylation ($v_{c,max}$) and maximum rate of electron transport (J_{max}) were measured under saturating light (1750 µmol PAR m^{-2} s^{-1}) from 150 Pa CO_2 to 5 Pa CO_2 with a flow rate of 200 µmol s^{-1}. Leaves stabilised at 150 Pa CO_2 at the measuring temperature for 30–40 min before decreasing CO_2 concentrations monotonically. This method was utilised to reduce the oscillations that occur under triose-phosphate utilisation limitation (McClain and Sharkey, 2023); however, this parameter could still not properly be fitted. $v_{c,max}$ and J_{max} were estimated using an R-based *ACi* fitting tool (Gregory et al., 2021) (see https://github.com/poales/msuRACiFit to access Rscript with user-friendly interface).

We used the Dynamic Assimilation Technique rather than using a steady-state method to generate the CO_2 response curves to facilitate measuring enough multiple temperatures in a reasonable amount of time. Response curves that utilise continuous ramping of CO_2 began with the Rapid A-C_i Response (RACiR) technique (Stinziano et al., 2017) paving the way for a more robust method (relative to the RACiR approach) based on re-deriving the equations for gas exchange for the non-steady state and implementing a range match to account for slight calibration differences between the sample and reference infrared gas analyzers (Saathoff and Welles, 2021). The speed in which the CO_2 response curves can be obtained (i.e., 5–7 min) compared to the traditional (i.e., 40–45 min) was especially important for measuring each genotype under a range of temperatures where we wanted to limit the plant's exposure to each condition.

2.9 | Calculating Lg_{tc}, Lg_m and WUE

Using the CO_2 response curves from above, Lg_{tc} and Lg_m were calculated at ambient CO_2 concentration (40–42 Pa CO_2). Lg_{tc} was calculated according to

$$L_{g_{tc}} = \frac{A_{sl} - A_n}{A_{sl}} \quad (7)$$

(Warren, 2004). Where A_n is the A that occurs at C_a 40–42 Pa CO_2 and A_{sl} (assuming no stomatal resistance) is the A that occurs when C_i 40–42 Pa CO_2. Lg_{tc} was calculated according to

$$L_{g_m} = \frac{A_{ml} - A_n}{A_{ml}}, \quad (8)$$

where A_{ml} (assuming stomatal but no mesophyll resistance) is the A that occurs when $C_c = C_i$ when C_a is 40–42 Pa CO_2. *WUE* was calculated from gas exchange measurements at 40 Pa CO_2 according to

$$WUE = \frac{A}{g_{sw}} \quad (9)$$

(Vialet-Chabrand et al., 2016).

2.10 | Preparing crude protein extract for protein quantification and enzymatic assays

Crude protein extracts were prepared from the youngest, fully expanded leaves of *R. stricta* and *N. tabacum*. Leaf punches were removed from *R. stricta* and *N. tabacum* using a cork borer (8.15 mm and 17 mm), immediately frozen in liquid N_2, and stored at −80°C. Leaf material was homogenise on ice with 1 mL of the Extraction buffer (50 mM EPPS buffer, pH 8.0, containing 1 mM EDTA, 10 mM DTT, 0.1% Triton X-100 [v/v], 0.5% polyvinylpyrrolidone, and 10 µL 1X SigmaFAST Protease Inhibitor Cocktail, EDTA Free (Sigma), using a 2 mL glass-to-glass homogeniser (Kontes Glass Co.). The homogenate was transferred into a 1.5 mL plastic Eppendorf tube and clarified by centrifugation for 10 min at 13 500*g* and 4°C (Eppendorf Centrifuge 5424R). The supernatant, containing the clarified crude protein extract, was used for protein quantification and enzyme assays.

2.11 | Protein quantification

Soluble protein content was determined in crude protein extract (Bio-Rad Protein Assay; BIO-RAD) according to the manufacturer instructions using a SpectraMax M2 Microplate Reader (Molecular Devices).

2.12 | Enzymatic assays

All enzyme activities were measured by spectrophotometric assays with the use of SpectraMax M2 Plate reader and SoftMax Pro7 software (Molecular Devices). PGP, GO, GGAT, AGAT, SGAT, HPR, and GLYK assays were performed in a 200 µL total reaction mix using polystyrene or acrylic UV transparent 96-well microplates (Corning), while the CAT assay was performed in 1 mL reaction mix using a quartz cuvette. The pH of reactions was selected based on the organellar pH where the reaction occurs (Heinze and Gerhardt, 2002; Kendziorek and Paszkowski, 2008; Liu et al., 2008; Shen et al., 2013). All enzyme assays were performed across two temperatures (25°C and 35°C) with three technical replicates. There were 4–5 independent biological replicates measured using leaf tissue from different plants.

2.13 | PGP activity

PGP activity was determined in *R. stricta* and *N. tabacum* colormetrically by the production of inorganic phosphate with the following modifications (Pai et al., 1990; Schwarte and Bauwe, 2007). 194 µL of reaction buffer (50 mM HEPES buffer, pH 7.5, 1 mM EDTA, and 10 mM $MgCl_2$) were combined with 4 µL of crude protein extract and 2 µL 200 mM 2-PG was added to initiate the reaction. The addition of the substrate was performed using a 96-well microplate replicator (Boekel). After 5 min the reaction was terminated by addition 32 µL of Pi reagent (2.5 N H_2SO_4, 0.2 mM antimony potassium tartrate, 4.9 mM ammonium molybdate, and 30 mM ascorbic acid). The plate was covered with parafilm, and the spectrophotometric readings were taken after 45 min at 880 µm using SpectraMax M2. To adjust for Pi that was produced independently from the PGP reaction, a control, containing reaction buffer and crude protein extract, was incubated for 5 min, then the reagent was added followed by 2-PG. A standard curve for Pi was constructed in the range 0.05–0.35 µg Pi per well using KH_2PO_4. PGP-specific activity was expressed in µmoles of 2-phosphoglycolate m^{-2} s^{-1}.

2.14 | Glycolate oxidase (GO) activity

The activity of GO was determined in *R. stricta* and *N. tabacum* by formation of glyoxylate phenylhydrazone (Baker and Tolbert, 1966; Zelitch et al., 2008) with the following modifications. The reaction mix contained 20 µL 0.5 mM K-phosphate buffer, pH 8.1, 10 µL of 110 mM phenylhydrazine, 10 µL 1.3 mM riboflavin, 3 µL crude protein extract, 152 µL sterile nQ water and 5 µL of 100 mM glycolic acid. The reaction was initiated with glycolic acid after the mix was pre-incubated for 5 min without the substrate. The addition of the substrate was performed with the use of a 96-well microplate replicator (Boekel). Control contained 5 µL water instead of the substrate. The increase in OD at 324 µm was measured in an acrylic UV transparent plate (Corning) for 5 min every 10 s. GO specific activity was calculated using the molar extinction coefficient of the glyoxylate-phenylhydrazone complex (17 mM^{-1} cm^{-1}) and expressed as µmol glyoxylate m^{-2} s^{-1}.

2.15 | CAT activity

The activity of CAT was determined in *R. stricta* and *N. tabacum* by the decomposition of H_2O_2 (Aebi, 1983; Zelitch, 1989) with the

following modifications. Small molecules from crude protein extract from both species were excluded using a Spin-X UF 500 10 K MWCO (Corning/Sigma-Aldrich, Inc.) protein concentrator cartridges to removes low molecular weight compounds, including specialised metabolites, which extensively absorb at 240 nm and interfere with the CAT assay. In brief, 300 µL crude protein extract and 200 µL extraction buffer with no PVDP were applied to the concentrator cartridge and centrifuged for 25 min, 15 000 rcf, 4°C. After centrifugation, an additional 200 µL of extraction buffer with no PVDP was added following another centrifugation under the same parameters. The extract from the concentrator cartridge was adjusted to 300 µL with extraction buffer with no PVDP before enzymatic assay so that CAT was not concentrated during this step. Since the concentrator membrane removes molecules up to 10 kDa and the molecular weight of CAT is approximately 60 kDa, CAT was not lost during this step and was not likely diluted or concentrated on a volume (or by extension, an area) basis. It is possible that soluble proteins lower than 10 kDa passed through the concentrator, resulting in an increase in CAT activities expressed on a protein basis. This protein loss was ~10% of the total soluble protein as determined by a Bradford assay.

The reaction mix containing 965.5 µL 50 mM K-phosphate buffer, pH 8.1, and 15 µL extract, was incubated for 1.5 min to determine the rate of background change in optical density. The reaction was initiated with 33.5 µL 30 mM H_2O_2 and the decline in optical density at 240 nm was observed for 1.5 min with 10 s intervals using spectrophotometer SpectraMax M2. The initial rate of reaction was determined during first 30 s and the specific activity was expressed as µmoles H_2O_2 m^{-2} s^{-1} using molar extinction coefficient for H_2O_2 at 240 nm 43.6 $M^{-1}cm^{-1}$.

2.16 | Glutamate glyoxylate aminotransferase (GGAT), alanine glyoxylate aminotransferase (AGAT), and serine glyoxylate aminotransferase (SGAT) activities

The activity of GGAT, AGAT, and SGAT were determined spectrophotometrically as described previously (Liepman & Olsen, 2001, 2003). Recombinant N-terminal 6xHis tagged HPR1 from *Arabidopsis thaliana* was used as a coupling enzyme in the assay for SGAT. HPR1 was produced in *Escherichia coli* LMG194 using a plasmid pBADAtHPR1 (obtained from S. Timm, University of Rostok), and the expression and purification of the enzyme were performed essentially as described previously (Liu et al., 2020). The specific activity of GGAT, AGAT, and SGAT were expressed in µmoles of (glutamate, alanine, and serine) m^{-2} s^{-1}.

2.17 | Hydroxypyruvate reductase (HPR) activity

The activity of HPR was determined in *R. stricta* and *N. tabacum* by the oxidation of NADH (Tolbert et al., 1970) with the following modifications. The reaction was initiated by adding 4 µL of 25 Na beta-hydroxypyruvate to the reaction mix, containing 192 µL of reaction buffer (100 mM K-phosphate buffer, pH 8.1, 0.15 mM NADH) and 4 µL crude extract. The addition of the substrate was performed with the use of a 96-well microplate replicator. The decrease in absorbance at 340 nm was monitored continuously for 5 min. To determine the rate of background utilisation of NADH, the controls contained 4 µL H_2O instead of the substrate. The specific activity of HPR was expressed in µmoles of hydroxypyruvate m^{-2} s^{-1}.

2.18 | Glycerate kinase (GLYK) activity

The activity of GK was determined by linking formation of 3-phosphoglycerate to NADH oxidation using a set of coupling enzymes identical to the set of coupling enzymes used for measuring rubisco activity (Walker et al., 2016b). 192 µL reaction buffer (containing 50 mM HEPES, pH 7.8, 10 mM $MgCl_2$, 60 mM KCl, 1 mM ATP, 0.2 mM NADH) (Kleczkowski & Randall, 1988) were combined with 4 µL crude protein extract, 4 µL coupling enzymes (22.5 U mL^{-1} 3-phosphoglycerate kinase, 250 U mL^{-1} carbonic anhydrase, 12.5 U mL^{-1} creatine phosphokinase, 20 U mL^{-1} glyceraldehyde-3-phosphate dehydrogenase, 20 U mL^{-1} glycerol-3-phosphate dehydrogenase, and 56 U mL^{-1} triose-phosphate isomerase), and the reaction was initiated by addition of 2 µL of 500 mM D-glycerate (5 mM final) (all from Sigma-Aldrich, Inc.); the substrate was added with the use of a 96-well microplate replicator. The decrease in optical density at 340 nm was monitored for 10 min. The initial rate of reaction was used to express the specific activity as µmoles glycerate m^{-2} s^{-1}.

2.19 | Data processing and statistical analyses

Gas exchange, stable carbon isotope, and biochemical data were visualised and analysed using custom scripts in R (R Core Team, 2021; RStudio Team, 2021). Student's *t*-test and repeated measures two-way analysis of variance (ANOVA) were used to measure significance ($p < 0.05$). All ANOVA tests were followed with Tukey's post hoc test. Additionally, all gas-exchange data followed the reporting format and recommendations defined in (Ely et al., 2021).

3 | RESULTS

3.1 | *R. stricta* performs higher photorespiration than *N. tabacum* under elevated temperatures

To assess the ability of *R. stricta* and *N. tabacum* to fix carbon under ambient photorespiratory conditions, the temperature response of v_o, v_o/v_c, A, and $A + R_L$ were measured under ambient O_2 conditions (21%) at low (250 µmol PAR m^{-2} s^{-1}) and high light (1750 µmol PAR m^{-2} s^{-1}) intensities (Figures 1 and 2). V_o in *R. stricta* was significantly

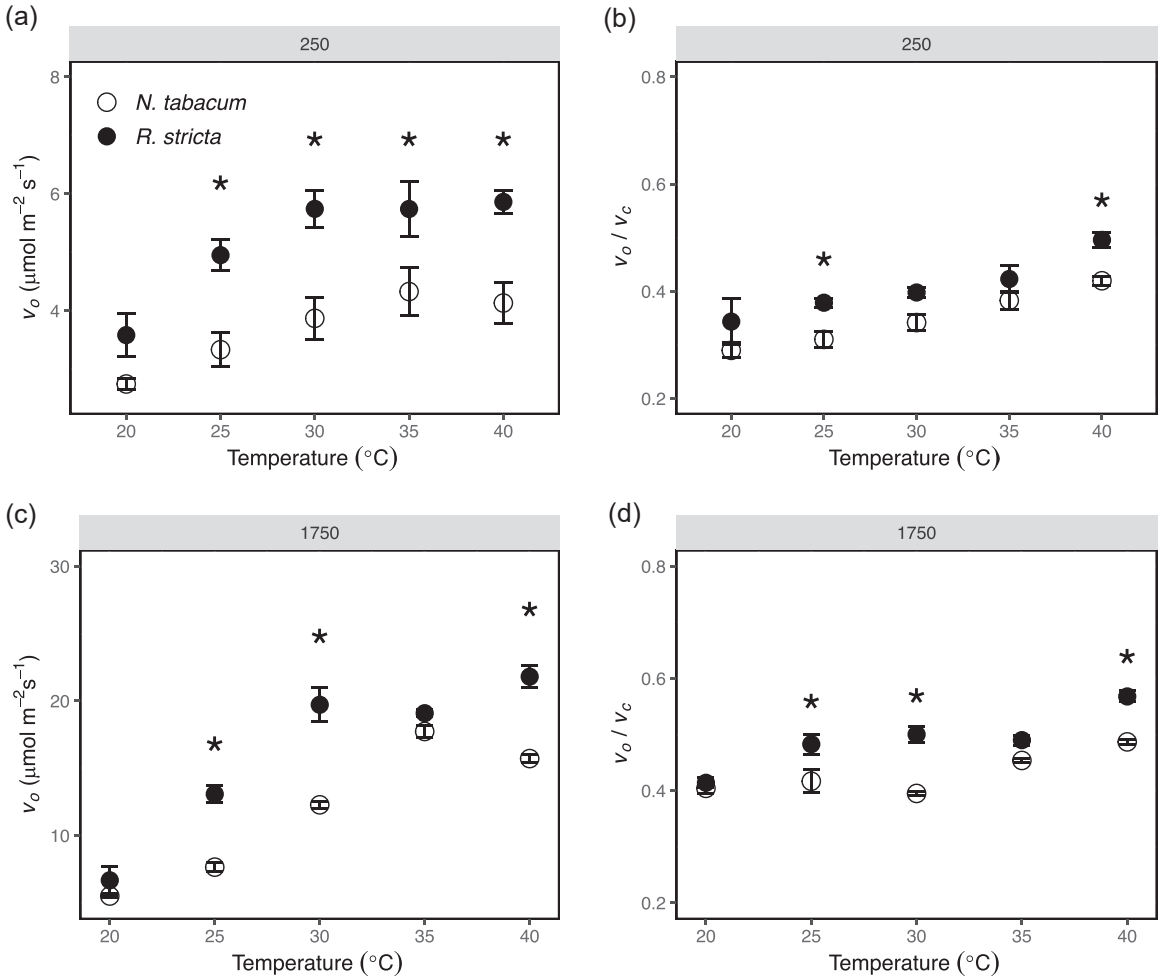

FIGURE 1 The temperature response of rubisco oxygenation rate in *Nicotiana tabacum* and *Rhazya stricta*. The temperature response of the oxygenation rate (v_o, a & c) and rubisco oxygenation per carboxylation (v_o/v_c, b & d) in *R. stricta* (closed symbols) and *N. tabacum* (open symbols). v_o and v_o/v_c were calculated from steady-state gas exchange measured under 40 Pa CO_2 and 250 or 1750 µmol PAR m^{-2} s^{-1}. Shown are the means of 4–5 biological replicates with ±SE bars. Significant difference between species is indicated by an asterisk as determined by two-way ANOVA with $p < 0.05$. ANOVA, analysis of variance; SE, standard error.

greater than *N. tabacum* at 25°C, 30°C, 35°C, and 40°C under low light and greater at 25°C, 30°C, and 40°C at high light (Figure 1a, c). At the growth temperature (~30°C), v_o in *R. stricta* was 48% (low light) and 60% (high light) greater than *N. tabacum*. The relative rate of rubisco oxygenation (v_o/v_c) in *R. stricta* was significantly greater than *N. tabacum* at 25°C and 40°C under low light and greater at 25°C, 30°C, and 40°C under high light (Figure 1b,d). The increased v_o and v_o/v_c in *R. stricta* indicate that rubisco catalysers oxygenation reactions more frequently than *N. tabacum* and therefore, experiences a greater photorespiratory pressure under most temperatures. *R. stricta* had similar rates of *A* to *N. tabacum* at 20°C, 25°C, 35°C, and 40°C; but a greater rate at 30°C under low light (Figure 2a). Under high light, *R. stricta* had similar rates of *A* as compared with *N. tabacum* at 20°C, 35°C, and 40°C; but a greater rate at 25°C and 30°C (Figure 2c). At the growth temperature, *A* in *R. stricta* was 20% (low light) and 16% (high light) larger than *N. tabacum*. R_L, which is needed to determine gross assimilation, was greater in *R. stricta* than *N. tabacum* at 20°C, 25°C, 30°C, 35°C, and 40°C (Supporting Information: Figure 1A). Gross assimilation was higher in *R. stricta* than *N. tabacum* at 25°C, 30°C, and 35°C under low light (Figure 2b). Under high light, gross assimilation in *R. stricta* was similar to *N. tabacum* at 20°C, 35°C, and 40°C; but greater at 25°C and 30°C (Figure 2d). These results indicate that the photosynthetic rate in *R. stricta* did not decrease despite high rates of photorespiration.

To understand *R. stricta* and *N. tabacum* abilities to fix carbon under minimal photorespiratory conditions, the temperature response of v_o, v_o/v_c, *A*, and $A + R_L$ were measured under low O_2 conditions and high light (2% 1750 PAR; Supporting Information: Figure 2). In contrast to the ambient O_2 conditions, v_o in *R. stricta* was similar to *N. tabacum* at 25°C and 40°C, but less than *N. tabacum* at 25°C, 30°C and 35°C (Supporting Information: Figure 1A). As expected, the rates of v_o in both species were reduced to a fraction of the 21% values under 2% O_2. v_o/v_c in *R. stricta* was similar to *N. tabacum* at 20°C, 25°C, 30°C, and 35°C, but greater than *N. tabacum* at 40°C (Supporting Information: Figure 1B). Under this

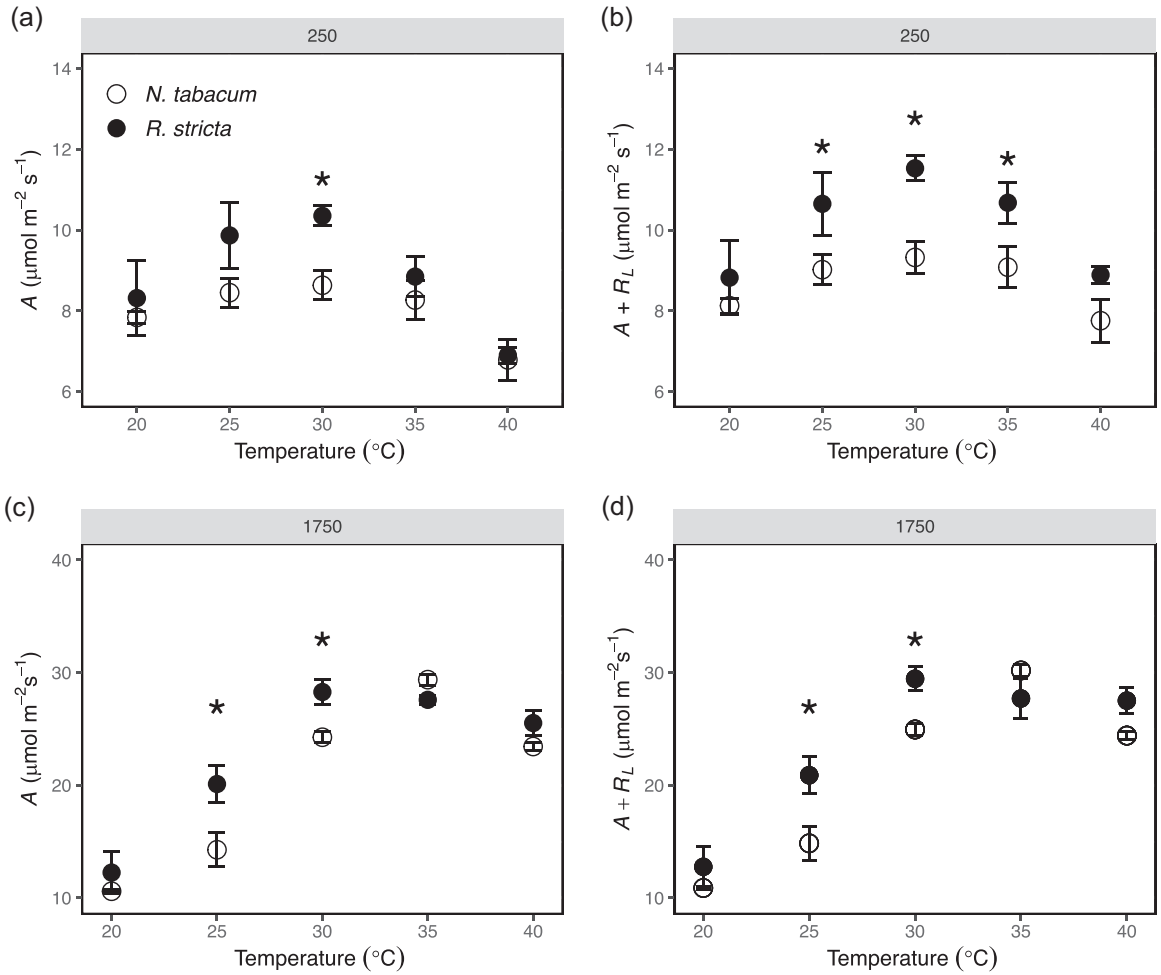

FIGURE 2 The temperature response of net and gross assimilation rates in *Nicotiana tabacum* and *Rhazya stricta*. The temperature response of net assimilation rate (*A*, a & c) and gross assimilation rate ($A + R_L$; b & d) in *R. stricta* (closed symbols) and *N. tabacum* (open symbols). *A* and $A + R_L$ were measured from steady-state gas exchange at 40 Pa CO_2 and 250 or 1750 μmol PAR m^{-2} s^{-1}. Shown are the means of four biological replicates with ±SE bars. Significant difference between species is indicated by an asterisk as determined by two-way ANOVA with $p < 0.05$. ANOVA, analysis of variance; SE, standard error.

minimal photorespiration, *R. stricta* had lower rates of *A* and $A + R_L$ than *N. tabacum* at 20°C, 25°C, 30°C, 35°C, and 40°C (Supporting Information: Figure 1C,D). The results indicate under minimal photorespiratory conditions, *R. stricta* ability to fix carbon is reduced compared to *N. tabacum*.

3.2 | Photosynthetic biochemical limitations of *R. stricta* and *N. tabacum*

To understand the biochemical limitations on photosynthesis, the temperature response of the J_{max} and the $v_{c,max}$ were estimated in *R. stricta* and *N. tabacum*. J_{max} in *R. stricta* was similar to *N. tabacum* at 20°C, but greater than *N. tabacum* at 25°C, 30°C, 35°C, and 40°C (Figure 3a). In contrast to J_{max}, $v_{c,max}$ did not have a consistent trend in *R. stricta*. $v_{c,max}$ in *R. stricta* was similar to *N. tabacum* at 20°C, greater than *N. tabacum* at 25°C, 30°C, and 40°C, but less than *N. tabacum* at 35°C.

To find the saturating light intensity and to understand photosynthetic capacity in *R. stricta* and *N. tabacum*, a light response curve was measured at 25°C (Supporting Information: Figure 3). Maximum quantum yield of CO_2 fixed per photon absorbed (Φ_{CO2}) was significantly greater in *R. stricta* (0.060 ± 0.0047) than *N. tabacum* (0.046 ± 0.0017) at 25°C.

Quantifying the photorespiratory CO_2 compensation point (Γ^*) under ambient O_2 conditions links rubisco kinetics with the stoichiometry of CO_2 release per rubisco oxygenation from photorespiration (Walker et al., 2016a). Additionally, the temperature response of Γ^* provides a key parameter needed to calculate v_o, v_c, and g_m. Γ^* in *R. stricta* was greater than *N. tabacum* at 30°C and 40°C, but similar to *N. tabacum* at 20°C, 25°C, and 35°C (Supporting Information: Figure 1B).

To understand whether differences in Γ^* are related to a variable or constant α between *R. stricta* and *N. tabacum*, we measured photorespiratory discrimination (Δ_f) and the $^{12}C/^{13}C$ fractionation during photorespiration (*f*). Interestingly, there was no significant

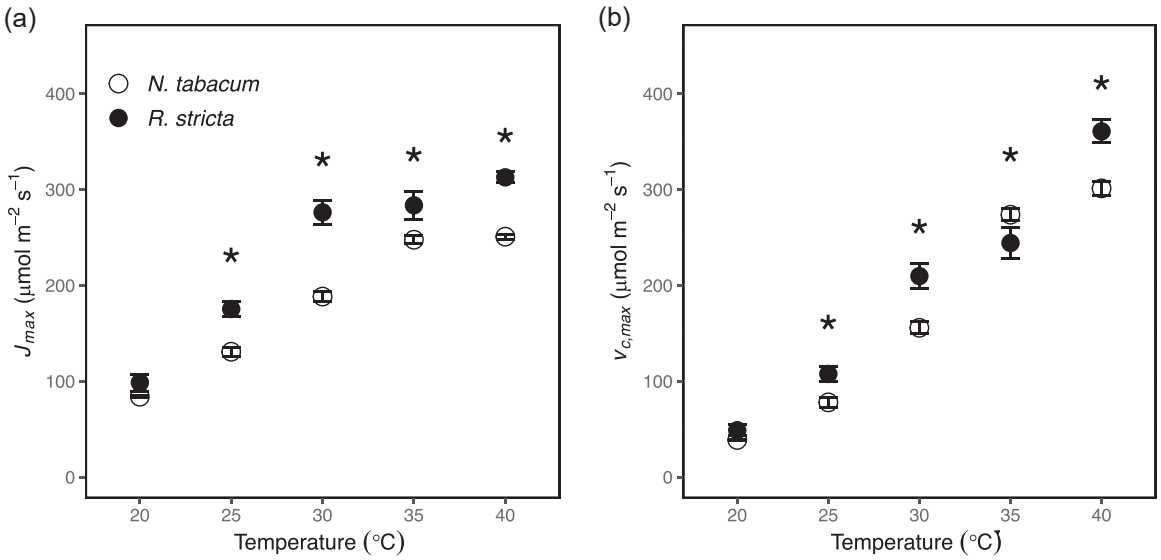

FIGURE 3 The temperature response of J_{max} and $v_{c,max}$ in *Nicotiana tabacum* and *Rhazya stricta*. The temperature response of the maximum rate of electron transport (J_{max}; a) and rubisco maximum carboxylation rates ($v_{c,max}$; b) in *R. stricta* (closed symbols) and *N. tabacum* (open symbols). J_{max} and $v_{c,max}$ were estimated from gas exchange measurements at 40–42 Pa CO_2 and 1750 µmol PAR m^{-2} s^{-1}. Shown are the means of four biological replicates with ±SE bars. Significant difference between species is indicated by an asterisk as determined by two-way ANOVA with $p < 0.05$. ANOVA, analysis of variance; SE, standard error.

difference between the species for either parameter at 25°C or 35°C (Supplemental Figure 4). To understand whether oxygen sensitivity in g_m lead to misinterpretation in Δ_f and f calculation, we measured at 2% and 21% oxygen at two key temperatures (25°C and 35°C) and determined no oxygen sensitivity to g_m using different assumptions for photorespiratory fractionation (Supporting Information: Figure 5).

3.3 | *R. stricta* partitions CO_2 transfer conductances for increased *WUE*

The temperature response of stomatal conductance and mesophyll conductance to CO_2 (g_{tc} and g_m) were measured to determine the CO_2 diffusion differences between *R. stricta* and *N. tabacum* (Figure 4a,c). g_{tc} was lower in *R. stricta* than *N. tabacum* at all temperatures. g_m in *R. stricta* was similar to *N. tabacum* at 20°C, 25°C, and 30°C, but greater at 35°C and 40°C. The results indicate that there is a tradeoff in the diffusive barriers in *R. stricta* from stomatal to mesophyll conductance.

The temperature response of the photosynthetic limitation imposed by stomatal conductance and mesophyll conductance to CO_2 (Lg_{tc} and Lg_m) were calculated to determine how much g_{tc} and g_m limit photosynthetic rate (Figure 4b,d). Lg_{tc} in *R. stricta* was greater than *N. tabacum* at 35°C, but similar to *N. tabacum* at the other temperatures. Lg_m in *R. stricta* was greater than *N. tabacum* at 25°C and 30°C, but similar to *N. tabacum* at the rest of the temperatures. Overall, g_{tc} and g_m did not impose a significant limitation of photosynthetic rate as Lg_{tc} and Lg_m did not have consistent trends across temperature for *R. stricta* or *N. tabacum*.

The temperature response of *WUE* was calculated to determine how the CO_2 transfer conductances constrained water use in *R. stricta* and *N. tabacum* (Supporting Information: Figure 6). *WUE* in *R. stricta* was greater compared with *N. tabacum* at 20°C, 25°C, 30°C, 35°C, and 40°C. The temperature response of WUE results indicate that *R. stricta* fixes carbon at a lower cost of water than *N. tabacum* on a stoichiometric basis.

3.4 | Photorespiratory enzyme activity in *R. stricta* compared with *N. tabacum*

We measured photorespiratory enzyme activities to determine which photorespiratory enzymes have higher activities and temperature responses in *R. stricta* as compared to *N. tabacum* (Figure 5). These enzymatic activities were measured in leaves in *R. stricta* and *N. tabacum* at 25°C and 35°C using crude protein extracts. The photorespiratory enzymes assayed PGP, GO, CAT, GGAT, AGAT, SGAT, HPR, and GLYK. *R. stricta* had greater PGP and CAT activities than *N. tabacum* at 25°C and 35°C. *R. stricta* had greater AGAT and SGAT activities than *N. tabacum* at 25°C. *R. stricta* had similar GO, GGAT, HPR, and GK activities to *N. tabacum* at 25°C and 35°C.

The temperature response ratio of the enzyme activities was calculated by dividing the activity per mg protein at 35°C by the activity per mg protein at 25°C for each enzyme to establish if there are greater enzyme activities (relative to 25°C) at the elevated temperature in *R. stricta* and *N. tabacum* (Supporting Information: Figure 7). PGP had a greater relative increase in activity with temperature in *R. stricta* as compared with *N. tabacum*; however, GO,

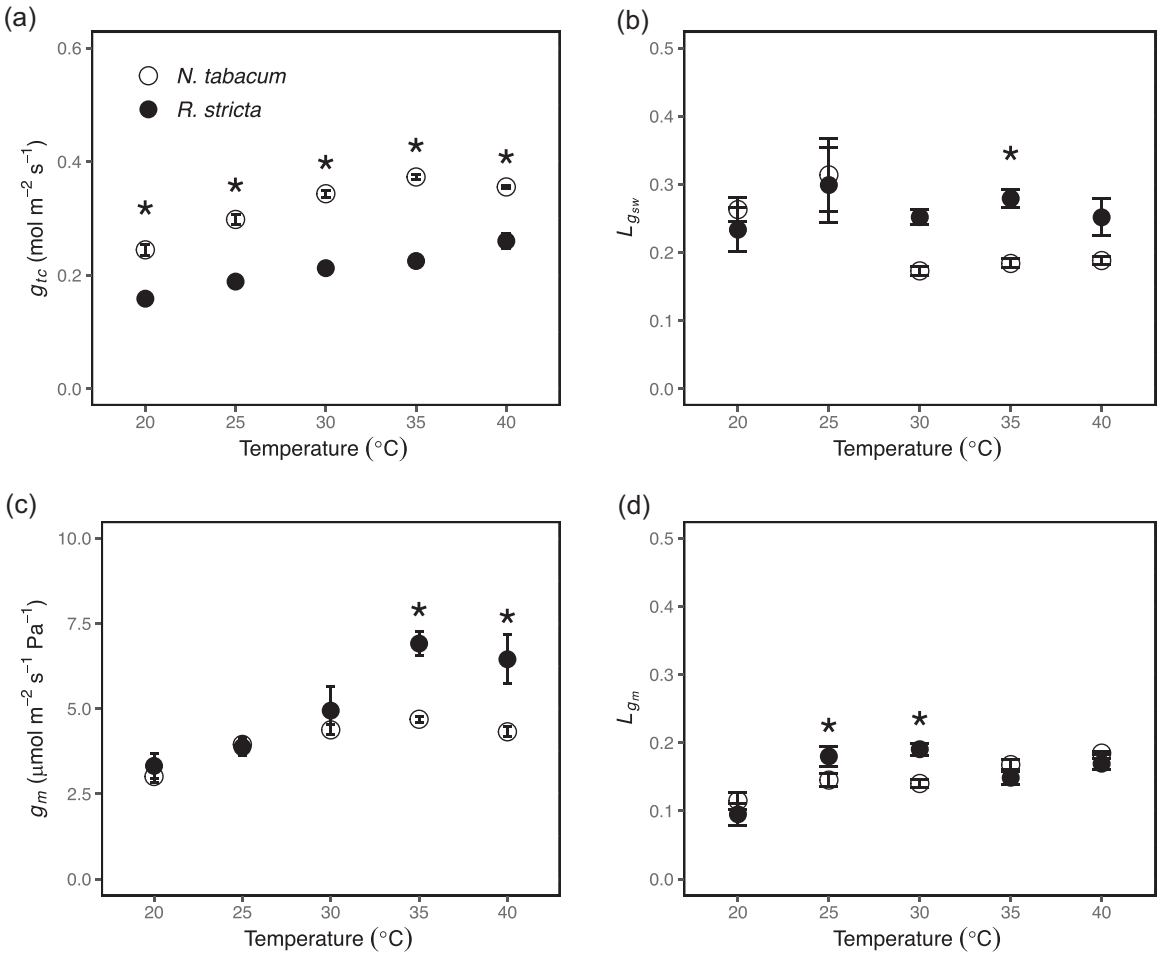

FIGURE 4 Temperature response of stomatal and mesophyll conductance and their limitations imposed on photosynthetic rate in *Nicotiana tabacum* and *Rhazya stricta*. The temperature response of stomatal conductance to CO_2 (g_{tc}; a), and mesophyll conductance to CO_2 (g_m; c) as well as the limitation imposed by both conductances (Lg_{tc} and Lg_m; b and d) *in R. stricta* (closed symbols) and *N. tabacum* (open symbols). g_{tc} and g_m were measured from steady-state gas exchange and on-line measurements of carbon isotope discrimination at 40 Pa CO_2 and 1750 µmol PAR m^{-2} s^{-1} (a & c). Lg_{tc} and Lg_m were estimated from gas exchange measurements at 40–42 Pa CO_2 and 1750 µmol PAR m^{-2} s^{-1}. Shown are the means of 4–5 biological replicates with ±SE bars. Significant difference between species is indicated by an asterisk as determined by two-way ANOVA with $p < 0.05$. ANOVA, analysis of variance; SE, standard error.

CAT, GGAT, AGAT, SGAT, HPR, and GLYK had similar temperature response ratios.

4 | DISCUSSION

4.1 | Hallmarks of a temperature-tolerant photorespiratory pathway

These results demonstrate that *R. stricta* maintains higher rates of photorespiration under moderate and elevated temperatures and that these higher rates of activity correlate with increased activity of key photorespiratory enzymes. The higher rates of photorespiration are evident in the temperature response of v_o and v_o/v_c, which were greater in *R. stricta* than in *N. tabacum* at moderate (25°C and 30°C) and elevated (35°C and 40°C) temperatures (Figure 1). Higher rates of photorespiration in *R. stricta* were accompanied by increased activities of specific photorespiratory enzymes. In *R. stricta*, PGP and CAT activities were greater than *N. tabacum* at 25°C and 35°C (Figure 5a,c). These higher photorespiratory enzyme activities in *R. stricta* compared with *N. tabacum* support the hypothesis that *R. stricta* has adapted to high photorespiratory pressure at moderate and elevated temperature by increased activity of these key enzymes. Additionally, the temperature response ratio of PGP activity in *R. stricta* was larger compared to *N. tabacum* (1.55 compared with 1.07; Supporting Information: Figure 7). The larger temperature response of PGP indicates a larger V_{max} in the *R. stricta* at elevated temperatures than *N. tabacum*. The larger temperature response of PGP at elevated temperatures could not be explained by gene expression differences between the species as these assays were conducted in vitro. However, the increase could result from a more thermostable isoform of PGP in *R. stricta* than *N. tabacum*.

Increased activity of PGP may allow photorespiration to maintain low concentrations of 2-PG, an inhibitor of C_3 cycle enzymes, that

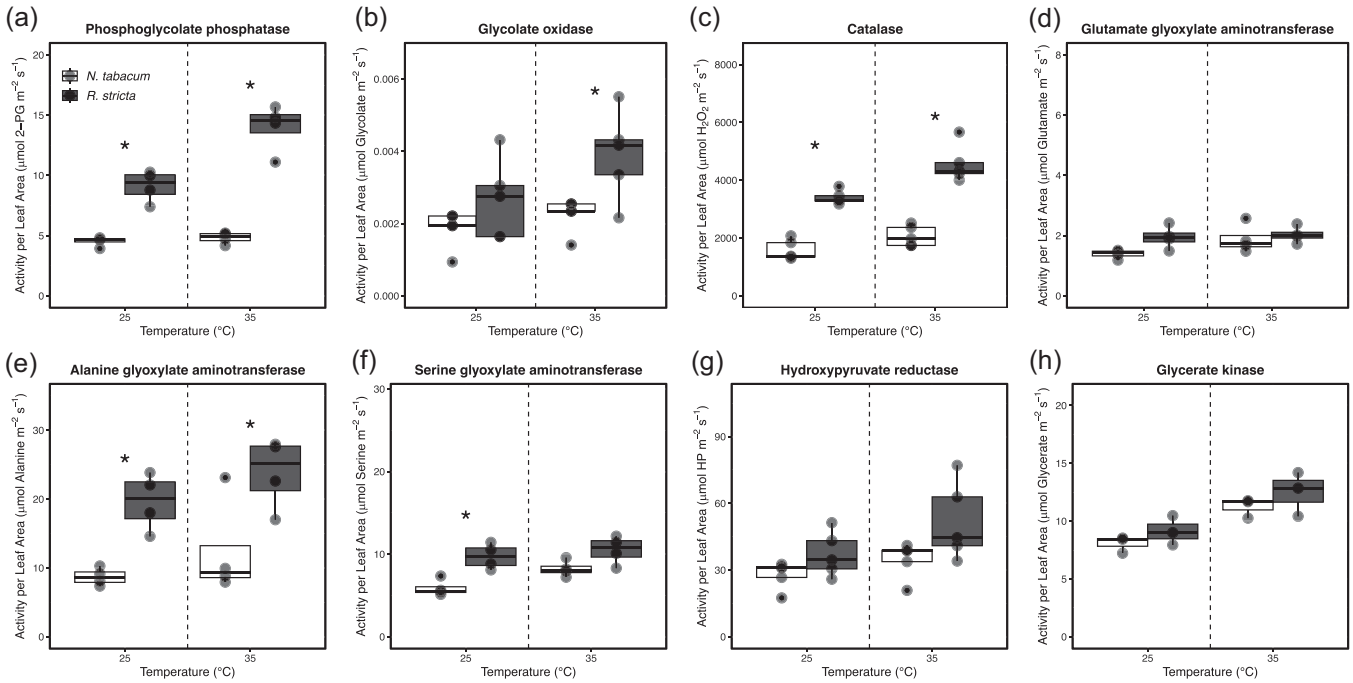

FIGURE 5 Photorespiratory enzymatic activities in *Nicotiana tabacum* and *Rhazya stricta* at 25°C and 35°C. Specific activities per m^2 leaf area were measured in *R. stricta* (black boxplot) and *N. tabacum* (white boxplot) using crude protein extracts for the enzymes phosphoglycolate phosphatase, glycolate oxidase, catalase, glutamate glyoxylate aminotransferase, alanine glyoxylate aminotransferase, serine glyoxylate aminotransferase, hydroxypyruvate reductase, and glycerate kinase. Shown are boxplots as well as points indicating the biological replicates. Significant difference between species is indicated by an asterisk as determined by Student's *t*-test with $p < 0.05$.

accumulates under moderate and elevated temperatures. Past work supports the hypothesis that efficient degradation of 2-PG by PGP is critical for maintaining high rates of photosynthesis under higher photorespiratory conditions. For example, *Arabidopsis* overexpressing PGP maintain higher photosynthetic rates after short-term and long-term exposure to elevated temperatures as compared to wild-type and maintain a lower steady-state pool of 2-PG (Flügel et al., 2017; Timm et al., 2019). Therefore, minimising the inhibition of photosynthesis by 2-PG appears to be a key feature for increasing the temperature resiliency of photorespiration in engineered and adapted plants.

CAT may also play a role in maintaining photosynthesis under higher photorespiratory pressure by detoxifying H_2O_2. Photorespiration is a large source of H_2O_2 in the light. H_2O_2 functions as a signalling molecule in both stress and developmental processes, where concentrations of H_2O_2 are likely under homoeostatic regulation by foliar-expressed CAT in the peroxisome (Dat et al., 2003; Queval et al., 2007; Queval et al., 2008). CAT-deficient *N. tabacum* has high concentrations of H_2O_2 that leads to cell death when plants were exposed to high photorespiratory pressure (Dat et al., 2003). Other work with CAT-deficient plants indicate the enzyme is an important mediator of cellular toxicity during environmental stress (Willekens, 1997). Additionally, there is evidence that H_2O_2 can react with glyoxylate and/or hydroxypyruvate resulting in nonenzymatic decarboxylation and release additional CO_2 from photorespiration (Cousins et al., 2008; Grodzinski, 1978; Halliwell & Butt, 1974; Keech et al., 2012; Zelitch, 1992). For example, in a mutant with reduced foliar-expressed CAT, photosynthetic rates are reduced due to an increase in the stoichiometry release of CO_2 per oxygenation, most likely from the nonenzymatic decarboxylation with hydroxypyruvate and H_2O_2 (Bao et al., 2021). This work supports the hypothesis that sufficient CAT activity plays a critical role preventing elevated H_2O_2 signalling and possibly the additional loss of CO_2 from photorespiration and is an adaptive strategy in *R. stricta* to moderate and elevated temperatures. Interestingly, we found no evidence that *N. tabacum* actually had an increase in CO_2 release per rubisco oxygenation as would be expected from excess nonenzymatic decarboxylations (discussed below). This finding indicates that the role of CAT in H_2O_2 signalling may be more important than any potential CO_2 loss from nonenzymatic decarboxylations.

Interestingly, when photorespiration was reduced under low O_2 conditions, both A and $A + R_L$ were lower in *R. stricta* compared to *N. tabacum* but were similar or slightly higher when measured under ambient O_2 conditions (Supporting Information: Figure 2 & Figure 2). The higher rates of A and $A + R_L$ in *N. tabacum* supports that the photorespiratory pathway in *R. stricta* reduces the inhibition of photosynthesis under photorespiratory conditions more efficiently than *N. tabacum*. In other words, A in *N. tabacum* is more sensitive to photorespiratory intermediates, despite having only half the rates of v_o. The increase in A and $A + R_L$ under photorespiratory conditions in *R. stricta* is therefore likely due to the greater activity of PGP and CAT in *R. stricta*, rather than an improved ability to fix carbon. These results also indicate that photosynthesis in *R. stricta* is adapted to environments with high photorespiratory pressure.

4.2 | Managing CO_2 transfer conductance for improved *WUE*

Our results demonstrate that *R. stricta* has a higher g_m that is compensated by a lower $g_{tc,}$ resulting in a similar overall CO_2 transfer conductance limitation to photosynthesis. *R. stricta* exhibits a lower g_{tc} than *N. tabacum* across the entire temperature gradient (Figure 5a). However, this conductance difference between *R. stricta* and *N. tabacum* does not impose a larger CO_2 limitation on photosynthetic rate (Figure 5b). *R. stricta* has a greater g_m than *N. tabacum* at elevated temperatures (Figure 5c). This difference in g_m at elevated temperatures does not reduce the CO_2 limitation on photosynthetic rate (Figure 5d). So why does this re-partitioning strategy exist in *R. stricta* if it does not support an increase in net CO_2 assimilation? *R. stricta* appears to have re-partitioned the CO_2 transfer conductance at high temperatures from the stomata, which loses water, to the mesophyll, which does not.

The implications of this re-partitioning of conductances result in *R. stricta* having an increase in *WUE*. Although the lower g_{tc} indicates that the initial CO_2 delivery into the leaf was more restricted in *R. stricta* than *N. tabacum*, it also means that water has a more restricted path leaving the leaf. The lower g_{tc} in *R. stricta* resulted in a greater *WUE* than *N. tabacum* (Supporting Information: Figure 6). The greater *WUE* indicates a lower cost of water loss per carbon assimilated, which is an important water-saving strategy. This water-saving strategy in *R. stricta* is consistent with other stomatal conductance measurements in other C_3 desert species, but the higher g_m has not yet been described to our knowledge (Driscoll et al., 2020; Driscoll et al., 2021; Kannenberg et al., 2021; Ogle et al., 2012).

4.3 | Other adaptive strategies of photosynthesis appear similar between species

Biochemical limitations of photosynthesis reveal key similarities and differences between *R. stricta* and *N. tabacum*. In *R. stricta*, the J_{max} was greater than *N. tabacum* at 25°C, 30°C, 35°C, and 40°C (Figure 3a). These higher rates of J_{max} in *R. stricta* are consistent with a higher photorespiratory capacity in *R. stricta*, since photorespiration dissipates more excitation energy from the electron transport chain than *N. tabacum* which would increase maximal rates of electron flux (Kozaki & Takeba, 1996).

In contrast to J_{max}, differences in $v_{c,max}$ were inconsistent between *R. stricta* and *N. tabacum*. In *R. stricta*, the $v_{c,max}$ was similar to *N. tabacum* at 20°C, and greater than *N. tabacum* at 25°C, 30°C, and 40°C (Figure 3a). Interestingly, $v_{c,max}$ in *R. stricta* was less than *N. tabacum* at 35°C. Generally, ignoring the 35°C data, there was a greater $v_{c,max}$ in *R. stricta* as temperature increased. Moreover, while we measured an increase in $v_{c,max}$ associated with temperature, others measure a $v_{c,max}$ independent of temperature in in situ studies of *R. stricta* (Lawson et al., 2014). Lawson et al. (2014) point to a potential thermostable rubisco activase as a potential strategy *R. stricta* uses to maintain rubisco catalytic capacity and activity at elevated temperatures. Potentially, this thermotolerant rubisco activase could be the reason we see higher $v_{c,max}$ in *R. stricta* compared with *N. tabacum* at 25°C, 30°C, and 40°C. However, we did not measure rubisco activity or activation state in this study.

Carbon assimilation is in part determined by the CO_2 released from R_L. Minimising R_L could be a strategy used by *R. stricta* to maintain a higher assimilation rate at elevated temperatures. Interestingly, R_L was greater in *R. stricta* compared to *N. tabacum* at each temperature (Supporting Information: Figure 1A). The higher R_L meant that *R. stricta* is respiring more non-photorespiratory CO_2 than *N. tabacum* in the light. When considering rates of carbon assimilation, *R. stricta* had higher *A* than *N. tabacum* at 30°C under low light and at 25°C and 30°C under high light. In contrast, when the CO_2 loss from R_L is added back, *R. stricta* maintained higher $A + R_L$ than *N. tabacum* at 25°C, 30°C, and 35°C under low light, and at 25°C and 30°C under high light, meaning that *R. stricta* fixed more carbon at these temperatures (Figure 2). Therefore, the greater rates of R_L in *R. stricta* reduce the amount of carbon fixed and does not explain why *R. stricta* can maintain higher *A* at growth temperatures (~30°C) under low or high light intensity than *N. tabacum*. This result demonstrates that minimising R_L does not appear to be a strategy that *R. stricta* uses to perform photosynthesis at higher rates compared with *N. tabacum* from a carbon budget perspective, but perhaps the elevated R_L contributes some yet-undescribed metabolic role in the elevated temperature tolerance.

Photosynthetic performance can also be characterised by Γ^* which links the specificity of rubisco for CO_2 over O_2 ($S_{c/o}$) to the stoichiometry of CO_2 release from rubisco oxygenation from photorespiration (α). A change in Γ^* may indicate differences in $S_{c/o}$ or α and may be an adaptive strategy in *R. stricta* to maintain photosynthetic performance. Interestingly, Γ^* was greater at 30°C and 40°C in *R. stricta* compared to *N. tabacum*, but similar at 20°C, 25°C, and 35°C. When considering changes in $S_{c/o}$, past work suggest that $S_{c/o}$ varies little within higher plants (Flamholz et al., 2019) but *R. stricta* was not included in this analysis, therefore not ruling out that it has adapted an improved $S_{c/o}$. Since the temperature response of Γ^* does not show any decrease in *R. stricta* as compared to *N. tabacum*, we do not see any evidence for adaptive changes in $S_{c/o}$ as a strategy that *R. stricta* uses to perform photosynthesis.

When considering α, previous work has resolved α to be 0.5 moles of CO_2 loss per rubisco oxygenation. The CO_2 loss is primarily attributed to the decarboxylation of glycine from the mitochondrion; however, if additional CO_2 is lost from NED in the peroxisome, the additional moles of CO_2 loss would be captured in this term. Determining α *in vivo* is difficult since it is integral to many of the simplifications and assumptions needed to interpret any gas exchange data in C_3 plants. For example, taken at face value, the Γ^* data would suggest that α actually increases in *R. stricta* as compared to *N. tabacum* which, if true, would mean that *R. stricta* has a less efficient photorespiratory pathway from a carbon balance perspective assuming a similar $S_{c/o}$. However, determining Γ^* requires assumptions of α to calculate Γ^* in the first place (i.e., g_m) clouding this interpretation. As an independent indicator to support the use of a constant α in all our calculations, we surmised that additional CO_2

release would carry a different isotopic fractionation since it would arise from a different reaction (not glycine decarboxylase). This is supported by past work indicating that the transgenic rice with reduced glycine decarboxylase activity (and more alternative decarboxylation reactions with a higher α) have greatly decreased f values from 16.2‰ to approximately 3.3‰ (Giuliani et al., 2019).

To determine if there was a decreased (or even different) f value consistent with a change in α, we measured Δ_f and f in *R. stricta* and *N. tabacum*. Interestingly, there was no significant difference between the species for either parameter at 25°C or 35°C (Supporting Information: Figure 4). Therefore, we do not see any evidence for differences in the reactions contributing to α between *R. stricta* and *N. tabacum*. Interestingly, there was an increase in R_L in *R. stricta* relative to *N. tabacum* but this can't be a reflection of a different α since this rate was not sensitive to different rates of photorespiration as indicated by the common intercept of the CO_2 response curves measured under different illumination during the common-intersection measurements. This approach cannot preclude a small rate of non-enzymatic decarboxylations or a reaction that has the same fractionation as glycine decarboxylation, but for the purposes of this study, we assume that $\alpha = 0.5$ for all the gas-exchange calculations. This assumption also suggests that the protection against these reactions by increased CAT expression may be accompanied by a self-regulating mechanism to down-regulate rubisco activity when CAT activity is too low to prevent them from happening, explaining why higher activities of CAT are important in *R. stricta*, but nonenzymatic decarboxylations do not appear to occur at high rates in *N. tabacum*.

Although *R. stricta* and *N. tabacum* share the same photosynthetic pathway (C_3 cycle), differences in Φ_{CO2} reveal changes in photosynthetic capacity (Supporting Information: Figure 3). At 25°C, *R. stricta* had a significantly greater Φ_{CO2} (0.060 ± 0.0047) than *N. tabacum* (0.046 ± 0.0017). The question arises: What occurs between light absorption by the antennae and the carboxylation of CO_2 by rubisco that allows *R. stricta* to maximise the number of CO_2 fixed per photon absorbed? Perhaps non-photochemical quenching and/or photosynthetic control through cytochrome b_6f is less, leading to a higher light use efficiency of photosystem II and higher electron transfer rates per photon absorbed (Eberhard et al., 2008). However, at low light absorption, we do not expect substantial non-photochemical quenching to occur in either species (Strand et al., 2023). To understand the differences in coupling between the light absorption and Φ_{CO2}, we would need more characterisations of the upstream light reactions in both species.

5 | CONCLUDING REMARKS

These results suggest important adaptive strategies used by *R. stricta* to maintain photosynthetic rates under moderate and elevated temperatures. To maintain high rates of photorespiration under most temperatures with minimal inhibitor accumulation, *R. stricta* increases photorespiratory capacity by reducing enzymatic bottlenecks. A second adaptive strategy in *R. stricta* to elevated temperatures is to increase water-use efficiency by lowering g_{tc} and increasing g_m. These strategies found in *R. stricta* may inform breeding and engineering efforts in other C_3 species to improve photosynthetic efficiency at elevated temperature.

ACKNOWLEDGMENTS

We would like to thank Dr. Salman Gulzar for help with *Rhazya stricta* cultivation and ecophysiology. We additionally thank Audrey Johnson for the valuable work and discussion during the cultivation process of *R. stricta*. We thank Deserah Strand for helpful discussion regarding Φ_{CO2} and potential adaptations in the light reaction pathway. We also thank Jim Klug and Cody Keilen (MSU Growth Chamber Facility) for overall greenhouse maintenance and pest management during plant cultivation. Finally, we would like to thank Hilary Stewart Williams for help setting up the tunable diode laser measurement system, including the software and hardware. L.M.G., L.V.R. and B.J.W. were funded by the Division of Chemical Sciences, Geosciences, and Biosciences, Office of Basic Energy Sciences of the United States Department of Energy (DE-FG02-91ER20021) and National Science Foundation awards from the Division of Integrative Organismal Systems (2030337).

DATA AVAILABILITY STATEMENT

The data that support the findings of this study are available from the corresponding author upon reasonable request.

ORCID

Berkley J. Walker http://orcid.org/0000-0001-5932-6468

REFERENCES

Abadie, C., Boex-Fontvieille, E.R.A., Carroll, A.J. & Tcherkez, G. (2016) In vivo stoichiometry of photorespiratory metabolism. *Nature Plants*, 2(2), 15220.

Aebi, H.E. (1983) Catalase. In: Bergmeyer, H.U., Ed. *Methods of enzymatic analysis*. Weinheim: Verlag Chemie. pp. 273–286.

Anderson, L.E. (1971) Chloroplast and cytoplasmic enzymes II. Pea leaf triose phosphate isomerases. *Biochimica et Biophysica Acta (BBA) - Enzymology*, 235(1), 237–244. https://doi.org/10.1016/0005-2744(71)90051-9

Baker, A.L. & Tolbert, N.E. (1966) Glycolate oxidase (ferredoxin containing form), *Methods in enzymology*, 9. Academic Press, pp. 339–342.

Bao, H., Morency, M., Rianti, W., Saeheng, S., Roje, S., Weber, A.P.M. et al. (2021) Catalase protects against nonenzymatic decarboxylations during photorespiration in *Arabidopsis thaliana*. *Plant Direct*, 5(12), e366. https://doi.org/10.1002/pld3.366

Barbour, M.M., McDowell, N.G., Tcherkez, G., Bickford, C.P. & Hanson, D.T. (2007) A new measurement technique reveals rapid post-illumination changes in the carbon isotope composition of leaf-respired CO_2. *Plant, Cell & Environment*, 30(4), 469–482. https://doi.org/10.1111/j.1365-3040.2007.01634.x

Bauwe, H., Hagemann, M., Kern, R. & Timm, S. (2012) Photorespiration has a dual origin and manifold links to central metabolism. *Current Opinion in Plant Biology*, 15(3), 269–275. https://doi.org/10.1016/j.pbi.2012.01.008

Von Caemmerer, S. (2000) *Biochemical models of leaf photosynthesis*. Csiro publishing.

von Caemmerer, S. & Evans, J.R. (2015) Temperature responses of mesophyll conductance differ greatly between species. *Plant, Cell &*

Environment, 38(4), 629–637. Available from: https://doi.org/10.1111/pce.12449

Cousins, A.B., Pracharoenwattana, I., Zhou, W., Smith, S.M. & Badger, M.R. (2008) Peroxisomal malate dehydrogenase is not essential for photorespiration in *Arabidopsis* but its absence causes an increase in the stoichiometry of photorespiratory CO_2 release. *Plant Physiology*, 148(2), 786–795. Available from: https://doi.org/10.1104/pp.108.122622

Dat, J.F., Pellinen, R., Van De Cotte, B., Langebartels, C., Kangasjärvi, J., Inzé, D. et al. (2003) Changes in hydrogen peroxide homeostasis trigger an active cell death process in tobacco. *The Plant Journal*, 33(4), 621–632. Available from: https://doi.org/10.1046/j.1365-313X.2003.01655.x

Driscoll, A.W., Bitter, N.Q. & Ehleringer, J.R. (2021) Interactions among intrinsic water-use efficiency and climate influence growth and flowering in a common desert shrub. *Oecologia*, 197(4), 1027–1038. Available from: https://doi.org/10.1007/s00442-020-04825-3

Driscoll, A.W., Bitter, N.Q., Sandquist, D.R. & Ehleringer, J.R. (2020) Multidecadal records of intrinsic water-use efficiency in the desert shrub *Encelia farinosa* reveal strong responses to climate change. *Proceedings of the National Academy of Sciences*, 117(31), 18161–18168. Available from: https://doi.org/10.1073/pnas.2008345117

Eberhard, S., Finazzi, G. & Wollman, F.A. (2008) The dynamics of photosynthesis. *Annual Review of Genetics*, 42, 463–515. Available from: https://doi.org/10.1146/annurev.genet.42.110807.091452

Ely, K.S., Rogers, A., Agarwal, D.A., Ainsworth, E.A., Albert, L.P., Ali, A. et al. (2021) A reporting format for leaf-level gas exchange data and metadata. *Ecological Informatics*, 61, 101232. Available from: https://doi.org/10.1016/j.ecoinf.2021.101232

Evans, J., Sharkey, T., Berry, J. & Farquhar, G. (1986) Carbon isotope discrimination measured concurrently with gas exchange to investigate CO_2 diffusion in leaves of higher plants. *Functional Plant Biology*, 13(2), 281–292. Available from: https://doi.org/10.1071/PP9860281

Evans, J.R. & von Caemmerer, S. (2013) Temperature response of carbon isotope discrimination and mesophyll conductance in tobacco. *Plant, Cell & Environment*, 36(4), 745–756. Available from: https://doi.org/10.1111/j.1365-3040.2012.02591.x

Farquhar, G.D. & Cernusak, L.A. (2012) Ternary effects on the gas exchange of isotopologues of carbon dioxide. *Plant, Cell & Environment*, 35(7), 1221–1231. Available from: https://doi.org/10.1111/j.1365-3040.2012.02484.x

Farquhar, G., O'Leary, M. & Berry, J. (1982) On the relationship between carbon isotope discrimination and the intercellular carbon dioxide concentration in leaves. *Functional Plant Biology*, 9(2), 121–137. Available from: https://doi.org/10.1071/PP9820121

Flamholz, A.I., Prywes, N., Moran, U., Davidi, D., Bar-On, Y.M., Oltrogge, L.M. et al. (2019) Revisiting trade-offs between rubisco kinetic parameters. *Biochemistry*, 58(31), 3365–3376. Available from: https://doi.org/10.1021/acs.biochem.9b00237

Flügel, F., Timm, S., Arrivault, S., Florian, A., Stitt, M., Fernie, A.R. et al. (2017) The photorespiratory metabolite 2-phosphoglycolate regulates photosynthesis and starch accumulation in arabidopsis. *The Plant Cell*, 29(10), 2537–2551. Available from: https://doi.org/10.1105/tpc.17.00256

Fu, X., Gregory, L.M., Weise, S.E. & Walker, B.J. (2023) Integrated flux and pool size analysis in plant central metabolism reveals unique roles of glycine and serine during photorespiration. *Nature Plants*, 9(1), 169–178. Available from: https://doi.org/10.1038/s41477-022-01294-9

Giuliani, R., Karki, S., Covshoff, S., Lin, H.-C., Coe, R.A., Koteyeva, N.K. et al. (2019) Knockdown of glycine decarboxylase complex alters photorespiratory carbon isotope fractionation in *Oryza sativa* leaves. *Journal of Experimental Botany*, 70(10), 2773–2786. Available from: https://doi.org/10.1093/jxb/erz083

Gregory, L.M., McClain, A.M., Kramer, D.M., Pardo, J.D., Smith, K.E., Tessmer, O.L. et al. (2021) The triose phosphate utilization limitation of photosynthetic rate: out of global models but important for leaf models. *Plant, Cell & Environment*, 44(10), 3223–3226. Available from: https://doi.org/10.1111/pce.14153

Grodzinski, B. (1978) Glyoxylate decarboxylation during photorespiration. *Planta*, 144(1), 31–37. Available from: https://doi.org/10.1007/BF00385004

Hall, N.P. & Keys, A.J. (1983) Temperature dependence of the enzymic carboxylation and oxygenation of ribulose 1, 5-bisphosphate in relation to effects of temperature on photosynthesis. *Plant Physiology*, 72(4), 945–948.

Halliwell, B. & Butt, V.S. (1974) Oxidative decarboxylation of glycollate and glyoxylate by leaf peroxisomes. *Biochemical Journal*, 138(2), 217–224. Available from: https://doi.org/10.1042/bj1380217

Heinze, M. & Gerhardt, B. (2002) Plant Catalases. In: Baker, A. & Graham, I.A., (Eds.) *Plant Peroxisomes: Biochemistry, Cell Biology And Biotechnological Applications*. Dordrecht: Springer Netherlands. pp. 103–140.

Hermida-Carrera, C., Kapralov, M.V. & Galmés, J. (2016) Rubisco catalytic properties and temperature response in crops. *Plant Physiology*, 171(4), 2549–2561. Available from: https://doi.org/10.1104/pp.16.01846

Jordan, D.B. & Ogren, W.L. (1984) The CO_2/O_2 specificity of ribulose 1,5-bisphosphate carboxylase/oxygenase. *Planta*, 161(4), 308–313. Available from: https://doi.org/10.1007/BF00398720

Kannenberg, S.A., Driscoll, A.W., Szejner, P., Anderegg, W.R.L. & Ehleringer, J.R. (2021) Rapid increases in shrubland and forest intrinsic water-use efficiency during an ongoing megadrought. *Proceedings of the National Academy of Sciences*, 118(52), e2118052118. Available from: https://doi.org/10.1073/pnas.2118052118

Keech, O., Zhou, W., Fenske, R., Colas-des-Francs-Small, C., Bussell, J.D., Badger, M.R. et al. (2012) The genetic dissection of a short-term response to low CO_2 supports the possibility for peroxide-mediated decarboxylation of photorespiratory intermediates in the peroxisome. *Molecular Plant*, 5(6), 1413–1416. Available from: https://doi.org/10.1093/mp/sss104

Kendziorek, M. & Paszkowski, A. (2008) Properties of serine:glyoxylate aminotransferase purified from *Arabidopsis thaliana* leaves. *Acta Biochimica et Biophysica Sinica*, 40(2), 102–110. Available from: https://doi.org/10.1111/j.1745-7270.2008.00383.x

Kleczkowski, L.A., & Randall, D.D. (1988) Substrate stereospecificity of leaf glycerate kinase from C3 and C4 plants. *Phytochemistry*, 27(5), 1269–1273. https://doi.org/10.1016/0031-9422(88)80176-6

Kozaki, A. & Takeba, G. (1996) Photorespiration protects C_3 plants from photooxidation. *Nature*, 384(6609), 557–560. Available from: https://doi.org/10.1038/384557a0

Kromdijk, J., Głowacka, K., Leonelli, L., Gabilly, S.T., Iwai, M., Niyogi, K.K. et al. (2016) Improving photosynthesis and crop productivity by accelerating recovery from photoprotection. *Science*, 354(6314), 857–861. Available from: https://doi.org/10.1126/science.aai8878

Laisk, A.K. (1977) Kinetics of photosynthesis and photorespiration of C_3 in plants, *Science*. Scientific Research, p. 195.

Larkindale, J. & Huang, B. (2004) Changes of lipid composition and saturation level in leaves and roots for heat-stressed and heat-acclimated creeping bentgrass (*Agrostis stolonifera*. *Environmental and Experimental Botany*, 51(1), 57–67. Available from: https://doi.org/10.1016/S0098-8472(03)00060-1

Lawrence, M.G. (2005) The relationship between relative humidity and the dewpoint temperature in moist air: a simple conversion and applications. *Bulletin of the American Meteorological Society*, 86(2), 225–234. Available from: https://doi.org/10.1175/bams-86-2-225

Lawson, T., Davey, P.A., Yates, S.A., Bechtold, U., Baeshen, M., Baeshen, N. et al. (2014) C_3 photosynthesis in the desert plant

Rhazya stricta is fully functional at high temperatures and light intensities. *New Phytologist*, 201(3), 862–873. Available from: https://doi.org/10.1111/nph.12559

Liepman, A.H. & Olsen, L.J. (2001) Peroxisomal alanine:glyoxylate aminotransferase (AGT1) is a photorespiratory enzyme with multiple substrates in *Arabidopsis thaliana*: AGT1, a peroxisomal photorespiratory transaminase. *The Plant Journal*, 25(5), 487–498. Available from: https://doi.org/10.1046/j.1365-313x.2001.00961.x

Liepman, A.H. & Olsen, L.J. (2003) Alanine aminotransferase homologs catalyze the glutamate:glyoxylate aminotransferase reaction in peroxisomes of *Arabidopsis*. *Plant Physiology*, 131(1), 215–227. Available from: https://doi.org/10.1104/pp.011460

Liu, L., Zhong, S., Yang, R., Hu, H., Yu, D., Zhu, D. et al. (2008) Expression, purification, and initial characterization of human alanine aminotransferase (ALT) isoenzyme 1 and 2 in high-five insect cells. *Protein Expression and Purification*, 60(2), 225–231. Available from: https://doi.org/10.1016/j.pep.2008.04.006

Liu, Y., Guérard, F., Hodges, M. & Jossier, M. (2020) Phosphomimetic T335D mutation of hydroxypyruvate reductase 1 modifies cofactor specificity and impacts arabidopsis growth in air. *Plant Physiology*, 183(1), 194–205. Available from: https://doi.org/10.1104/pp.19.01225

Marcum, K.B. (1998) Cell membrane thermostability and whole-plant heat tolerance of Kentucky bluegrass. *Crop Science*, 38(5), 1214–1218. https://doi.org/10.2135/cropsci1998.0011183X003800050017x

McClain, A.M. & Sharkey, T.D. (2023) Rapid CO_2 changes cause oscillations in photosynthesis that implicate PSI acceptor-side limitations. *Journal of Experimental Botany*, 74, 3163–3173. https://doi.org/10.1093/jxb/erad084

Moore, C.E., Meacham-Hensold, K., Lemonnier, P., Slattery, R.A., Benjamin, C., Bernacchi, C.J. et al. (2021) The effect of increasing temperature on crop photosynthesis: from enzymes to ecosystems. *Journal of Experimental Botany*, 72(8), 2822–2844. Available from: https://doi.org/10.1093/jxb/erab090

Ogle, K., Lucas, R.W., Bentley, L.P., Cable, J.M., Barron-Gafford, G.A., Griffith, A. et al. (2012) Differential daytime and night-time stomatal behavior in plants from North American deserts. *New Phytologist*, 194(2), 464–476. Available from: https://doi.org/10.1111/j.1469-8137.2012.04068.x

Pai, S.-C., Yang, C.-C., & Riley, J. P. (1990) Effects of acidity and molybdate concentration on the kinetics of the formation of the phosphoantimonylmolybdenum blue complex. *Analytica Chimica Acta*, 229, 115–120.

Pörtner, H.O., Roberts, D.C., Tignor, M., Poloczanska, E.S., Mintenbeck, K. & Alegría, A. (eds.) (2022) *IPCC, 2022: Climate Change 2022: Impacts, Adaptation, and Vulnerability*. Cambridge Univeristy Press.

Prasertthai, P., Paethaisong, W., Theerakulpisut, P. & Dongsansuk, A. (2022) High temperature alters leaf lipid membrane composition associated with photochemistry of PSII and membrane thermostability in rice seedlings. *Plants*, 11(11), 1454. Available from: https://doi.org/10.3390/plants11111454

Queval, G., Hager, J., Gakiere, B. & Noctor, G. (2008) Why are literature data for H_2O_2 contents so variable? A discussion of potential difficulties in the quantitative assay of leaf extracts. *Journal of Experimental Botany*, 59(2), 135–146. Available from: https://doi.org/10.1093/jxb/erm193

Queval, G., Issakidis-Bourguet, E., Hoeberichts, F.A., Vandorpe, M., Gakière, B., Vanacker, H. et al. (2007) Conditional oxidative stress responses in the *Arabidopsis* photorespiratory mutant CAT2 demonstrate that redox state is a key modulator of daylength-dependent gene expression, and define photoperiod as a crucial factor in the regulation of H_2O_2-induced cell death. *The Plant Journal: For Cell and Molecular Biology*, 52(4), 640–657. Available from: https://doi.org/10.1111/j.1365-313X.2007.03263.x

R Core Team. (2021) *R: A language and environment for statistical computing*. Vienna, Austria: R Foundation for Statistical Computing. Retrieved from https://www.R-project.org

Rawson, H.M., Begg, J.E. & Woodward, R.G. (1977) The effect of atmospheric humidity on photosynthesis, transpiration and water use efficiency of leaves of several plant species. *Planta*, 134(1), 5–10. Available from: https://doi.org/10.1007/BF00390086

RStudio Team. (2021) *RStudio: integrated development environment for R*. Boston, MA: RStudio, PBC. Retrieved from http://www.rstudio.com/

Saathoff, A.J. & Welles, J. (2021) Gas exchange measurements in the unsteady state. *Plant, Cell & Environment*, 44(11), 3509–3523. Available from: https://doi.org/10.1111/pce.14178

Schwarte, S. & Bauwe, H. (2007) Identification of the photorespiratory 2-phosphoglycolate phosphatase, PGLP1, in arabidopsis. *Plant Physiology*, 144(3), 1580–1586. Available from: https://doi.org/10.1104/pp.107.099192

Shen, J., Zeng, Y., Zhuang, X., Sun, L., Yao, X., Pimpl, P. et al. (2013) Organelle pH in the *Arabidopsis* endomembrane system. *Molecular Plant*, 6(5), 1419–1437. Available from: https://doi.org/10.1093/mp/sst079

Somerville, C.R. (2001) An early *Arabidopsis* demonstration. Resolving a few issues concerning photorespiration. *Plant Physiology*, 125(1), 20–24.

Somerville, C.R. & Ogren, W.L. (1980) Photorespiration mutants of *Arabidopsis thaliana* deficient in serine-glyoxylate aminotransferase activity. *Proceedings of the National Academy of Sciences*, 77(5), 2684–2687.

South, P.F., Cavanagh, A.P., Lopez-Calcagno, P.E., Raines, C.A. & Ort, D.R. (2018) Optimizing photorespiration for improved crop productivity. *Journal of Integrative Plant Biology*, 60(12), 1217–1230. Available from: https://doi.org/10.1111/jipb.12709

De Souza, A.P., Burgess, S.J., Doran, L., Hansen, J., Manukyan, L., Maryn, N. et al. (2022) Soybean photosynthesis and crop yield are improved by accelerating recovery from photoprotection. *Science*, 377(6608), 851–854. Available from: https://doi.org/10.1126/science.adc9831

Stinziano, J.R., Morgan, P.B., Lynch, D.J., Saathoff, A.J., McDermitt, D.K. & Hanson, D.T. (2017) The rapid A–Ci response: photosynthesis in the phenomic era. *Plant, Cell & Environment*, 40(8), 1256–1262. Available from: https://doi.org/10.1111/pce.12911

Strand, D.D., Karcher, D., Ruf, S., Schadach, A., Schöttler, M.A., Sandoval-Ibañez, O. et al. (2023) Characterization of mutants deficient in N-terminal phosphorylation of the chloroplast ATP synthase subunit β. *Plant Physiology*, 191(3), 1818–1835. Available from: https://doi.org/10.1093/plphys/kiad013

Tazoe, Y., von Caemmerer, S., Estavillo, G.M. & Evans, J.R. (2011) Using tunable diode laser spectroscopy to measure carbon isotope discrimination and mesophyll conductance to CO_2 diffusion dynamically at different CO_2 concentrations. *Plant, Cell & Environment*, 34(4), 580–591. Available from: https://doi.org/10.1111/j.1365-3040.2010.02264.x

Tcherkez, G. (2006) Viewpoint: how large is the carbon isotope fractionation of the photorespiratory enzyme glycine decarboxylase? *Functional Plant Biology*, 33(10), 911–920. Available from: https://doi.org/10.1071/FP06098

Timm, S., Woitschach, F., Heise, C., Hagemann, M. & Bauwe, H. (2019) Faster removal of 2-phosphoglycolate through photorespiration improves abiotic stress tolerance of arabidopsis. *Plants*, 8(12), 563. Available from: https://doi.org/10.3390/plants8120563

Tolbert, N.E., Yamazaki, R.K. & Oeser, A. (1970) Localization and properties of hydroxypyruvate and glyoxylate reductases in spinach leaf particles. *Journal of Biological Chemistry*, 245(19), 5129–5136. Available from: https://doi.org/10.1016/S0021-9258(18)62827-3

Ubierna, N., Holloway-Phillips, M.-M. & Farquhar, G.D. (2018) Using stable carbon isotopes to study C3 and C4 photosynthesis: models and calculations. In: Covshoff, S., (Ed.) *Photosynthesis: methods and protocols*. New York, NY: Springer New York. pp. 155–196.

Urban, J., Ingwers, M., McGuire, M.A. & Teskey, R.O. (2017a) Stomatal conductance increases with rising temperature. *Plant Signaling & Behavior*, 12(8), e1356534. Available from: https://doi.org/10.1080/15592324.2017.1356534

Urban, J., Ingwers, M.W., McGuire, M.A. & Teskey, R.O. (2017b) Increase in leaf temperature opens stomata and decouples net photosynthesis from stomatal conductance in *Pinus taeda* and *Populus deltoides* x nigra. *Journal of Experimental Botany*, 68(7), 1757–1767. Available from: https://doi.org/10.1093/jxb/erx052

Vialet-Chabrand, S., Matthews, J.S.A., Brendel, O., Blatt, M.R., Wang, Y., Hills, A. et al. (2016) Modelling water use efficiency in a dynamic environment: an example using *Arabidopsis thaliana*. *Plant Science*, 251, 65–74. Available from: https://doi.org/10.1016/j.plantsci.2016.06.016

Walker, B.J. & Cousins, A.B. (2013) Influence of temperature on measurements of the CO_2 compensation point: differences between the Laisk and O_2-exchange methods. *Journal of Experimental Botany*, 64(7), 1893–1905. Available from: https://doi.org/10.1093/jxb/ert058

Walker, B.J., Kramer, D.M., Fisher, N. & Fu, X. (2020) Flexibility in the energy balancing network of photosynthesis enables safe operation under changing environmental conditions. *Plants*, 9(3), 301. Retrieved from https://www.mdpi.com/2223-7747/9/3/301

Walker, B.J., Skabelund, D.C., Busch, F.A. & Ort, D.R. (2016a) An improved approach for measuring the impact of multiple CO_2 conductances on the apparent photorespiratory CO_2 compensation point through slope–intercept regression. *Plant, Cell & Environment*, 39(6), 1198–1203. Available from: https://doi.org/10.1111/pce.12722

Walker, B.J., South, P.F. & Ort, D.R. (2016b) Physiological evidence for plasticity in glycolate/glycerate transport during photorespiration. *Photosynthesis Research*, 129(1), 93–103. Available from: https://doi.org/10.1007/s11120-016-0277-3

Warren, C.R. (2004) The photosynthetic limitation posed by internal conductance to CO_2 movement is increased by nutrient supply. *Journal of Experimental Botany*, 55(406), 2313–2321. Available from: https://doi.org/10.1093/jxb/erh239

Willekens, H. (1997) Catalase is a sink for H_2O_2 and is indispensable for stress defence in C3 plants. *The EMBO Journal*, 16(16), 4806–4816. Available from: https://doi.org/10.1093/emboj/16.16.4806

Yates, S.A., Chernukhin, I., Alvarez-Fernandez, R., Bechtold, U., Baeshen, M., Baeshen, N. et al. (2014) The temporal foliar transcriptome of the perennial C3 desert plant Rhazya stricta in its natural environment. *BMC Plant Biology*, 14(1), 1–22. https://doi.org/10.1186/1471-2229-14-2

Zelitch, I. (1989) Selection and characterization of tobacco plants with novel O2-Resistant photosynthesis. *Plant Physiology*, 90(4), 1457–1464. Available from: https://doi.org/10.1104/pp.90.4.1457

Zelitch, I. (1992) Factors affecting expression of enhanced catalase activity in a tobacco mutant with O_2-resistant photosynthesis. *Plant Physiology*, 98(4), 1330–1335. Available from: https://doi.org/10.1104/pp.98.4.1330

Zelitch, I., Schultes, N.P., Peterson, R.B., Brown, P. & Brutnell, T.P. (2008) High glycolate oxidase activity is required for survival of maize in normal air. *Plant Physiology*, 149(1), 195–204. Available from: https://doi.org/10.1104/pp.108.128439

SUPPORTING INFORMATION

Additional supporting information can be found online in the Supporting Information section at the end of this article.

How to cite this article: Gregory, L.M., Roze, L.V. & Walker, B.J. (2023) Increased activity of core photorespiratory enzymes and CO_2 transfer conductances are associated with higher and more optimal photosynthetic rates under elevated temperatures in the extremophile *Rhazya stricta*. *Plant, Cell & Environment*, 46, 3704–3720. https://doi.org/10.1111/pce.14711